Communication

Paraffin-Based RF Microsystems for Millimeter-Wave Reconfigurable Antenna

Behnam Ghassemiparvin and Nima Ghalichechian

***Abstract*— We report the design, fabrication, and testing of a millimeter-wave (mmW) reconfigurable antenna based on paraffin phase change material (PCM) variable capacitors. Paraffin is a low-loss dielectric ($\tan\delta = 6.6 \times 10^{-4}$ at 100 GHz) that undergoes a 15% volumetric change through its solid–liquid phase change. A radio frequency (RF) electrothermomechanical actuator is monolithically integrated with a slot antenna in order to achieve a frequency reconfiguration at 100 GHz. RF performance is verified using on-wafer probing and compared with full-wave and multiphysics simulations. The measured bandwidth of 94.1–104.1 GHz and the resonance frequency shift of 6.8 GHz are achieved. With a maximum voltage of 5.4 V, paraffin-based electrothermomechanical actuators have a maximum displacement of 1.4 μm, which yielded a 15.3% capacitance change. Using a fully coupled multiphysics simulation, switching time of the actuator is estimated as 5.7 ms. This work is the first demonstration for the new class of low-loss reconfigurable RF microsystem that will enable applications, including wireless communication, radars, and biomedical sensing.**

***Index Terms*— Millimeter wave (mmW), paraffin, phase change material (PCM), reconfigurable antenna, slot antenna.**

I. Introduction

The recent advent of media-rich mobile devices has increased the demand for high-data-rate wireless millimeter-wave (mmW) communications. Such systems, with their very high bandwidth in the frequency range of 30–300 GHz, can accommodate this rapid increase in traffic volume. The advent of both the Internet of Things and the increasing number and volume of connected devices has made data traffic both random and diverse. The introduction of frequency, polarization, or pattern diversity through multiple-input–multiple-output (MIMO) systems also increases the capacity of an mmW communication system. Currently, full potential of MIMO performance is not realized in mmW systems due to the limited radio frequency (RF) chains and sparse communication channel [1]. Reconfigurability and adaptability offer an additional degree of freedom for mmW communication systems to achieve optimal transmission. Using single reconfigurable antenna, it is possible to meet various radiation patterns, frequencies, and polarization requirements without increasing the number of elements and the associated RF chains. We note that the realization of reconfigurable antennas at the mmW band provides significant challenges in the design, fabrication, and testing steps.

Manuscript received February 24, 2020; revised July 12, 2021; accepted July 13, 2021. Date of publication August 9, 2021; date of current version January 11, 2022. This work was supported in part by the U.S. National Science Foundation under Grant 1408228 and Grant 1845370. *(Corresponding author: Nima Ghalichechian.)*

Behnam Ghassemiparvin was with the ElectroScience Laboratory, Department of Electrical and Computer Engineering, The Ohio State University, Columbus, OH 43212 USA. He is now with Apple Inc., Cupertino, CA 95014 USA (e-mail: ghassemiparvin.1@osu.edu).

Nima Ghalichechian was with the ElectroScience Laboratory, Department of Electrical and Computer Engineering, The Ohio State University, Columbus, OH 43212 USA. He is now with the School of Electrical and Computer Engineering, Georgia Institute of Technology, Atlanta, GA 30332 USA (e-mail: nima.1@gatech.edu).

Color versions of one or more figures in this communication are available at https://doi.org/10.1109/TAP.2021.3102112.

Digital Object Identifier 10.1109/TAP.2021.3102112

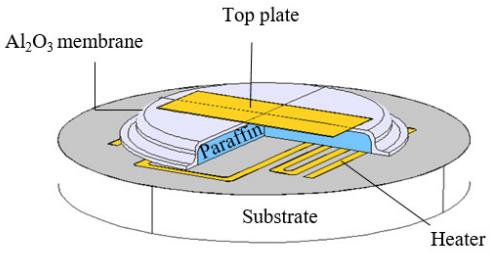

Fig. 1. 3-D schematic of the paraffin PCM actuator with integrated heater.

Altering the current distribution of an antenna makes it possible to reconfigure the radiation characteristics and input impedance. Various methods are used for such configuration: electrically tunable elements such as p-i-n diodes [2]–[5], varactors [6], [7], gallium-arsenide (GaAs) switches [8], and RF microelectromechanical systems (MEMS) [9], [10]. Alternatively, it is possible to achieve reconfiguration by using electrically tunable dielectric materials such as liquid crystals [11], [12] and barium strontium titanate (BST) [13] can also be used.

Paraffin or alkane is a mechanical phase change material (PCM) with a 15% density change over the solid-to-liquid phase transition [14], [15]. Thermomechanical actuators based on paraffin can simultaneously provide a large force and displacement [16]–[18]. In addition, the nonpolar molecular structure of paraffin yields a low dielectric loss of 6.3×10^{-4} at 110 GHz [19], which facilitates the development of low-loss RF components.

Using this unique combination of features, in this communication, we detail our development of a slot antenna with two low-loss paraffin-based variable capacitors to achieve a frequency reconfiguration at 100 GHz. The basic operation of this paraffin PCM-based variable capacitor, a 3-D schematic of which is shown in Fig. 1, is as follows. A dc voltage is first applied to the integrated heater to provide the electrothermal actuation. The generated heat then increases the temperature of the paraffin, with the resulting phase change from solid to liquid. Consequently, volume expansion of the paraffin provides the force to move the top plate of the capacitor. By loading the slot antenna with these capacitors, we can vary both the capacitance and the propagation constant along the slot line to achieve a resonance frequency shift. We base this concept upon our previously published design variations and preliminary simulation results [20]–[22].

This work is the first demonstration of the paraffin-based reconfigurable mmW antenna that is capable of continuous tuning. The proposed paraffin-based reconfigurable PCM capacitors offer a viable solution for low loss, monolithically integrated devices that could realize reconfigurable antennas at mmW frequencies. In our previous work [23], MEMS design of the paraffin PCM capacitor and mechanical and thermal challenges of the device is discussed. In addition, full description of the microfabrication process and the multiphysics simulation of the electrothermomechanical actuation is presented.

0018-926X © 2021 IEEE. Personal use is permitted, but republication/redistribution requires IEEE permission.
See https://www.ieee.org/publications/rights/index.html for more information.

Authorized licensed use limited to: Georgia Institute of Technology. Downloaded on January 12,2022 at 13:54:24 UTC from IEEE Xplore. Restrictions apply.

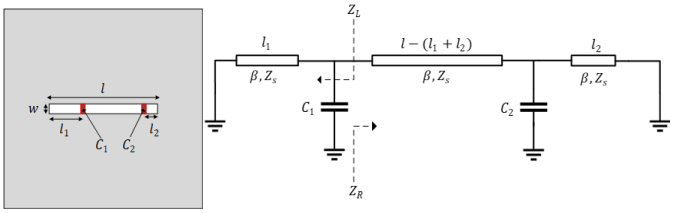

(a) (b)

Fig. 2. (a) Schematic of a loaded slot antenna and (b) equivalent transmission line model.

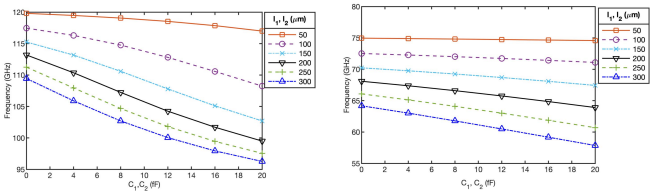

(a) (b)

Fig. 3. Calculated (a) first and (b) second resonance frequencies of the slot antenna with the length of 1357 μm and width of 80 μm fabricated on a 200 μm-thick quartz substrate with a relative dielectric constant of 3.8.

On the other hand, in this communication, we have focused on the antenna design, feeding structure, and the integration of the paraffin PCM capacitors with the mmW slot antenna. In addition, RF characterization of the variable capacitor integrated with the antenna is performed. Moreover, the effects of the microfabrication tolerances and the mechanical performance of the device on the electromagnetic losses and the reconfigurability are addressed.

II. Reconfigurable Slot Antenna Design

To determine the physical dimension of antenna, capacitance values, and location, we used a transmission line model of the antenna. Using this model, the resonance frequency of the antenna is calculated and the capacitors value and location were optimized to achieve maximum frequency shift with respect to capacitance change.

A. Circuit Model and Optimization of Loaded Slot Antenna

A narrow slot antenna can be modeled as a transmission line shorted at two ends. This circuit is at resonance when the length of the slot is $l = n(\lambda/2)$ where $n = 1, 2, 3, \ldots$ [24]. Loading this transmission line with two capacitors increases the capacitance and the propagation constant along the line. Consequently, electrical length of the antenna increases and the resonance frequency decreases [7], [25], [26]. Similar to [25] and [26], the transmission line model of the loaded slot antenna is used, as shown in Fig. 2. Using the circuit model, we then calculate the resonance frequency of the antenna by applying the transverse resonance condition [27]. Using similar analysis to [26], the resonance frequency of the loaded slot antenna is calculated, which is dependent on the capacitor values and their location.

Our objective is to maximize the frequency shift with respect to the capacitance ratio of 1.15. This capacitance ratio is determined according to the 15% volumetric change of paraffin. Due to the symmetric structure of the antenna, here, it is assumed that $l_1 = l_2$ and $C_1 = C_2$. The optimization procedure is applied for a slot antenna with the length of 1357 μm and the width of 80 μm fabricated on a 200 μm-thick quartz substrate with a relative dielectric constant of 3.8. For the capacitance range of $0 \leq C_1 = C_2 \leq 20$ fF, we vary the position of capacitors in the range of 50 μm $\leq l_1 = l_2 \leq$ 300 μm. The calculated resonance frequencies are shown in Fig. 3.

According to Fig. 3(a), the maximum rate of change for the first resonance is 0.32 GHz/fF, which occurs at $l_1 = l_2 = 300$ μm. The rate of change for the second resonance frequency is given in Table I where the maximum rate of 1.39 GHz/fF is achieved for $l_1 = l_2 =$ 200 μm. As the rate of change for second resonance frequency is significantly higher than the first, we consider only the second resonance frequency for the antenna design. In addition, second resonance is advantageous because its electric field distribution along the slot has two maximum points that are ideal locations for capacitive loading. Furthermore, due to the higher operation frequency of second resonance, small changes in the capacitance result in higher reactive loading variations.

TABLE I

Rate of Change of the Second Resonance Frequency With Respect to the Change in Capacitance for Capacitor Position in the Range of 50–300 μm

l_1, l_2 (μm)	50	100	150	200	250	300
$\Delta f_{R2}/\Delta C$ (GHz/fF)	0.28	0.93	1.28	1.39	1.38	1.32

Note that the calculated resonance frequencies using the circuit model are only an approximation since the effects of radiation, feed network, and finite ground size are not considered. The purpose of this model is only to determine the approximate value and the capacitor locations. Therefore, full-wave simulation is used to characterize the exact resonance frequency.

B. Radiation Pattern of the Reconfigurable Slot Antenna

The radiation pattern of a slot antenna depends on the electric field (magnetic current) distribution over its aperture [24], [25]. The slot antenna at its first resonance has a symmetric field distribution, which results in a broadside radiation pattern. On the other hand, at its second resonance, field distribution is antisymmetric, which creates null at the broadside [25]. The bent slot antenna mentioned in [26] was designed for the operation in the microwave band with p-i-n diodes used for the frequency reconfiguration. We have adopted and modified this bent slot design for operation at 100 GHz and reconfiguration using paraffin variable capacitors. Since the antenna is operated at its second resonance, geometry of the antenna is modified as a bent slot. A bending of the antenna causes cancellation of magnetic currents in the bent section, which yields a field distribution similar to the first resonance. Hence, the antenna will have a broadside radiation pattern [25].

III. Full-Wave Simulation of the Reconfigurable Slot Antenna

The geometry of the designed reconfigurable slot antenna is shown in Fig. 4. The bent slot has a width of 80 μm and a total length of 1357 μm, which is approximately one wavelength at 130 GHz. The antenna substrate is a 200 μm-thick quartz with a relative dielectric constant of $\epsilon_r = 3.8$ and a loss tangent of 4×10^{-4}. The ground plane of the antenna is 2.2×3.4 mm^2 and it is fabricated with a 750 nm-thick (three times the skin depth at 100 GHz) layer of gold with the conductivity of 4.1×10^7 S/m. Full-wave simulation is performed using ANSYS HFSS.

The slot antenna is loaded with paraffin PCM capacitors and the PCM device, as shown in Fig. 1, consists of a Joule heater positioned under the ground plane to ensure a minimum electromagnetic coupling to the antenna. The initial thickness of the paraffin is considered

Authorized licensed use limited to: Georgia Institute of Technology. Downloaded on January 12,2022 at 13:54:24 UTC from IEEE Xplore. Restrictions apply.

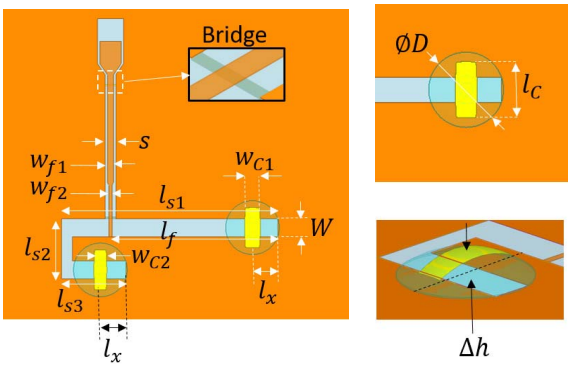

Fig. 4. 3-D simulation model of the reconfigurable antenna. Detailed view of (a) antenna and (b) paraffin PCM capacitor.

TABLE II

GEOMETRIC PARAMETERS OF ANTENNAS, CAPACITORS, AND FEED LINES IN MICRONS

l_{s1}	l_{s2}	l_{s3}	W	l_f	S	w_{f1}	w_{f2}	w_{ab}
964	268	285	80	746	47	14	27	8

l_x	w_{C1}	w_{C2}	l_C	D	h
113	58	70	200	120	2.6

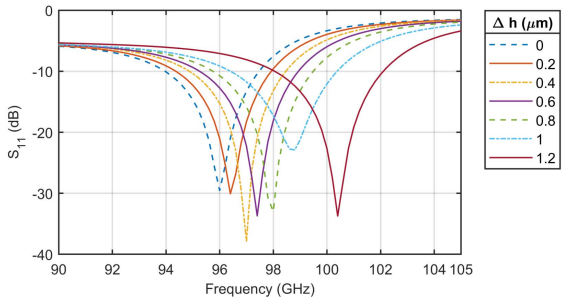

Fig. 5. Simulated S_{11} of the antenna with respect to center displacement of the paraffin PCM capacitor.

as 2.6 μm with a maximum center displacement of 1.2 μm, which is determined using multiphysics simulation [23]. The relative dielectric constant and the loss tangent of paraffin are 2.55 and 6.3×10^{-4} [19], respectively. Although the approximate values for the capacitance and their locations are calculated in Section II-A, the exact values for the width of capacitor top plate, w_{C1} and w_{C2}, are determined using a full-wave simulation, as given in Table II.

The slot antenna is fed through an off-center coplanar waveguide (CPW) transmission line where the input impedance at the feed location is 118 Ω. The antenna is impedance-matched to 50 Ω using a quarter-wave transformer. To avoid parasitic slot line modes at the transition points on the transmission lines, air bridges are used [28]. These air bridges are fabricated under the CPW lines and separated by a 1 μm-thick layer of silicon dioxide ($\epsilon_r = 2.2$) rather than being suspended in air. All of the dimensions of the antenna are given in Table II.

Fig. 5 shows the simulated return loss of the antenna with respect to the maximum displacement. The total reconfigured antenna bandwidth is 94–102.2 GHz ($S_{11} < -10$ dB) and the resonance frequency (minimum of S_{11}) changes by 4.6 GHz. Increasing the

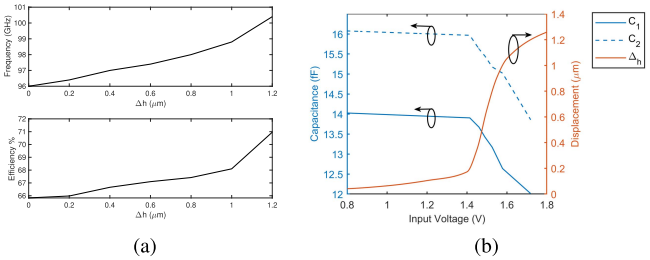

Fig. 6. (a) Resonance frequency and total efficiency with respect to the center displacement of the capacitor. (b) Capacitance change and maximum center displacement of the paraffin PCM capacitor for various input voltages.

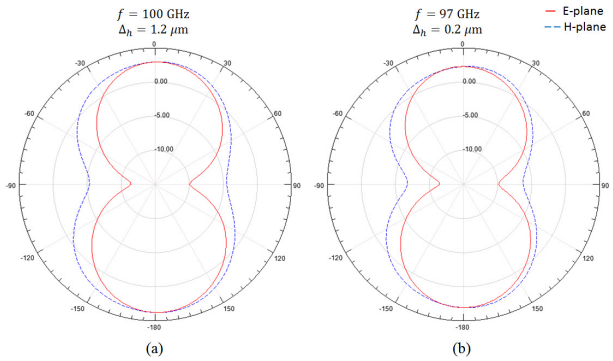

Fig. 7. Principal plane patterns of the reconfigurable antenna for the center displacement of (a) 1.2 μm at 100 GHz and (b) 0.2 μm at 97 GHz.

displacement results in a decrease in capacitance, which increases the resonance frequency, as shown in Fig. 6(a). The antenna efficiency at resonance frequency with respect to the displacement is shown in Fig. 6(b). It can be observed that a decrease in resonance frequency also decreases the radiation efficiency as a result of the reduction in the electrical size of the antenna [29]–[31].

A lumped element model is next used to characterize the capacitance and the loss of the paraffin PCM device. Using the full-wave simulation, paraffin PCM capacitors are replaced with lumped ports and three-port S-parameters of the antenna are determined. Next, S-parameters are imported into a circuit simulator and the series capacitance and resistance are extracted. A plot of the extracted capacitance value versus the input heater voltage is shown in Fig. 6(b). The results of these full-wave and multiphysics simulations resulted in a capacitance change of 15.3% for the maximum displacement of 1.2 μm, which is consistent with the volumetric expansion of the paraffin. The average series resistance of the paraffin PCM capacitor is found to be 610 mΩ.

The simulated radiation pattern of the antenna for the center displacement of 1.2 and 0.2 μm is shown in Fig. 7. Since the current distribution for different displacement values is approximately constant, antenna maintains its bidirectional pattern and has a maximum realized gain of 3 dBi at 100 GHz.

IV. EXPERIMENTAL RESULTS

The antenna integrated with paraffin PCM capacitors is fabricated using a six-layer photolithography process as described in [23]. Note that the fabrication paraffin PCM actuator is compatible with surface micromachining processes that can be implemented similar to the conventional MEMS process. A micrograph of the fabricated antenna and the paraffin PCM capacitor is shown in Fig. 8.

The 3-D profile measurement results of the mechanical displacement of the paraffin actuator are illustrated in [23] where the

Authorized licensed use limited to: Georgia Institute of Technology. Downloaded on January 12,2022 at 13:54:24 UTC from IEEE Xplore. Restrictions apply.

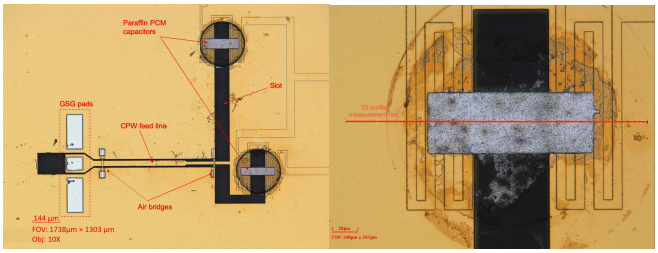

(a) (b)

Fig. 8. Micrograph of the fabricated (a) reconfigurable slot antenna and (b) paraffin PCM capacitor.

maximum displacement at the center of the device is to be 1.4 μm with an initial paraffin film thickness of 2.6 μm. Moreover, based on the transient multiphysics simulation, the switching time to actuate the device is 5.7 ms [23].

Using a ground–signal–ground (GSG) mmW probe, the input impedance of the antenna is characterized. Based on this measurement, reconfiguration capability and the RF performance of paraffin PCM capacitor are evaluated. Our measurement setup consists of a waveguide probe (Form Factor Inc.) connected to a frequency extender (Virginia Diodes Inc.), combined with a PNA (Keysight N5242A). The frequency range of the setup is limited to 90–140 GHz. A probe station was used for the experiments with a 30 mm-thick foam layer to isolate the wafer from the metallic chuck (see Fig. 9 for an illustration of this measurement configuration). The foam layer is approximately 10λ thick, which minimizes the effect of the metallic chuck on the impedance of the antenna.

One-port calibration is performed in two steps. Initially, the network analyzer is calibrated to a reference plane at the output of the frequency extender. Short, $\lambda/8$-delayed short and load standards are used for this calibration. After attaching the probe to the waveguide port, the system is calibrated to the reference place at the tip of the probe. Calibration is performed using on-wafer, four CPW offset shorts [36]. The CPW dimensions are 10/96/10 μm and the length of the lines is determined using established methods in [37] and [38]. A micrograph of the calibration standards is shown in Fig. 10. For the first short, the contact point of the probe is 350 μm away from the shorting plane to minimize the effect of the probe-CPW discontinuity, with the probe pads that are designed to match the 100 μm probe pitch. The short standards have a delay length difference of 200 μm that corresponds to 83° at 110 GHz.

Both PCM capacitors are excited by applying the dc voltage of 1–6 V to heaters in series configuration. DC voltage is supplied using a dc source (Keysight B2901A) via separate probes. Reflection coefficient of the antenna is measured for various heater voltages. The arrangement of the probes is shown in the inset of Fig. 9.

The antenna reflection coefficient with an input voltage of zero yields an antenna resonance frequency of 94.6 GHz, as shown in Fig. 11(a). Using the lumped element model based on the full-wave simulation (described in Section III), it is calculated that $C_1 = 17.8$ fF and $C_2 = 25.3$ fF with an estimated resistance value of 4.4 Ω. Measured resistance values are significantly higher than the simulated value of 610 mΩ given in Section III. Increased resistance could be due to extreme rough surface and the variation of the thickness of the fabricated aluminum layer. In addition, losses in the simulated antenna model could be underestimated, and in this case, contribution of all of the losses is reflected in the PCM capacitors. To actuate the capacitors, 5.4 V is applied to the heaters and the reflection coefficient

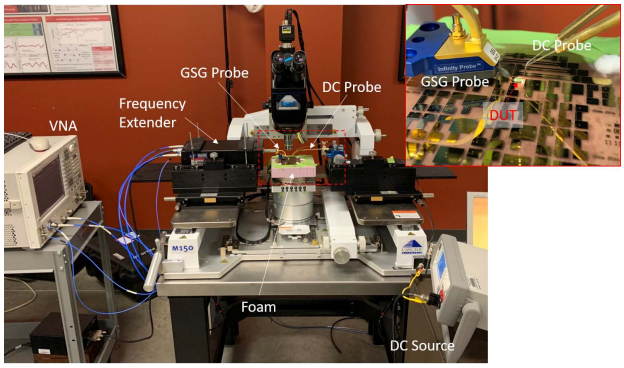

Fig. 9. mmW measurement setup. Close-up view of the probes and the device under test (DUT) is shown in the inset.

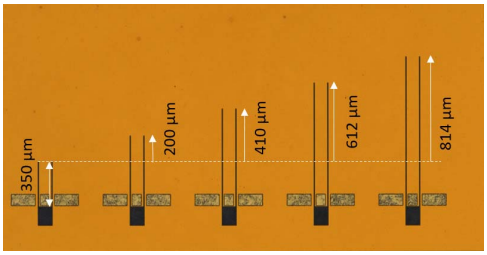

Fig. 10. Micrograph of the CPW offset short calibration standards.

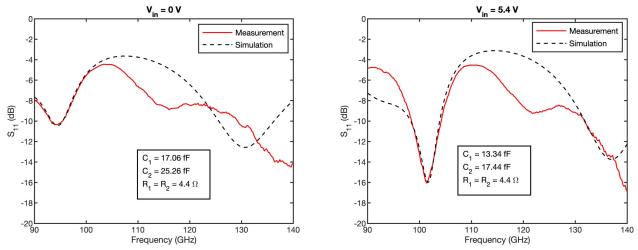

(a) (b)

Fig. 11. Comparison of the simulated and measured S_{11} of the antenna for heater voltage of (a) 0 and (b) 5.4 V.

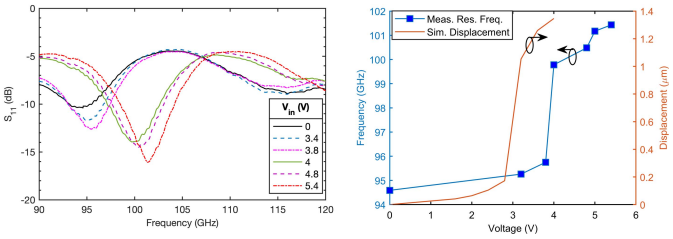

(a) (b)

Fig. 12. Measured (a) reflection coefficient and (b) resonance frequency (frequency of maximum return loss) of the antenna and the simulated displacement of the paraffin PCM capacitor with respect to the input voltage of the heater [23].

of the antenna is shown in Fig. 11(b). Extracted capacitance values are $C_1 = 13.4$ fF and $C_2 = 17.4$.

Fig. 12(a) shows S_{11} of the antenna for input heater voltage of 0–5.4 V. An antenna covers the bandwidth of 94.1–104.1 GHz. In Fig. 12(b), the resonance frequency is shown as a function of voltage of the heater. Resonance frequency increases monotonically

Authorized licensed use limited to: Georgia Institute of Technology. Downloaded on January 12,2022 at 13:54:24 UTC from IEEE Xplore. Restrictions apply.

TABLE III
COMPARISON OF mmW RECONFIGURABLE ANTENNAS IN THE LITERATURE

Reference	Reconfiguring element	No. of elements	No. of states	Variable change (%)	Frequency range	Frequency shift
[32]	PIN diode switched capacitor	1	Discrete	Capacitance, 59% (63–100 fF)	27.8–28.8 GHz	1 GHz
[33]	Schottky varactor	1	Continuous	Capacitance, 100% (2.4–4.79 fF)	202.7–197 GHz	5.7 GHz
[34]	Pneumatic actuator	1	Continuous	Displacement, 187%, (200–573 μm)	51–55.3 GHz	4.3 GHz
[10]	RF-MEMS	2	4	N/A	28, 29.2, 31.5, 35 GHz	7 GHz
[35]	Photoconductive switch	4	2	N/A	30, 34 GHz	4 GHz
This work	Paraffin PCM Capacitor	2	Continuous	Capacitance, 15%	94.3–101.6 GHz	7.3 GHz

from 94.3 to 101.6 GHz. As the voltage increases from 3.8 to 4 V, we observe a rapid increase in the resonance frequency, which is associated with phase transition of the paraffin. Based on the multiphysics simulation, by controlling the input voltage of the heater, fine-tuning can be achieved. However, since the current design does not include any packaging, the temperature distribution of the capacitor is highly dependent on the ambient.

A comparison of our novel design with state-of-the-art mmW reconfigurable antennas from the literature is given in Table III. It can be observed that the paraffin PCM-based reconfigurable antenna can achieve a reconfiguration range of 7.3 GHz with a relatively small capacitance change of 15%.

V. CONCLUSION

A continuously reconfigurable mmW slot antenna using paraffin PCM variable capacitors was designed, fabricated, and tested. To achieve reconfiguration, a bent slot antenna is loaded with two PCM variable capacitors. This work is the first implementation of an mmW reconfigurable antenna using a class of electrothermally actuated capacitor based on the paraffin PCMs, which is capable of operation at 100 GHz. Unique combination of low dielectric loss and large temperature-dependent density change of paraffin facilitates the development of low-loss reconfigurable structures at mmW band. In contrast to the classical RF-MEMS devices, paraffin PCM variable capacitors offer continuous tuning with a similar low-loss performance with a series resistance of less than 0.7 Ω at 100 GHz.

Using on-wafer probe measurements, it was shown that the designed reconfigurable antenna covers the bandwidth of 94.1–104.1 GHz and the resonance frequency shifts from 94.3 to 101.6 GHz with the increasing heater voltage. In addition, the capacitance change of the paraffin PCM devices is calculated to be 15.3% for a measured maximum displacement of 1.34 μm. The antenna has a simulated maximum gain of 3 dBi. A good agreement is observed between the simulation and measurement results for both electromagnetic performance of the antenna and displacement of the capacitor.

REFERENCES

[1] B. He and H. Jafarkhani, "Low-complexity reconfigurable MIMO for millimeter wave communications," *IEEE Trans. Commun.*, vol. 66, no. 11, pp. 5278–5291, Nov. 2018.

[2] D. Peroulis, K. Sarabandi, and L. P. B. Katehi, "Design of reconfigurable slot antennas," *IEEE Trans. Antennas Propag.*, vol. 53, no. 2, pp. 645–654, Feb. 2005.

[3] S. Genovesi, A. D. Candia, and A. Monorchio, "Compact and low profile frequency agile antenna for multistandard wireless communication systems," *IEEE Trans. Antennas Propag.*, vol. 62, no. 3, pp. 1019–1026, Mar. 2014.

[4] Y. P. Selvam, L. Elumalai, M. G. N. Alsath, M. Kanagasabai, S. Subbaraj, and S. Kingsly, "Novel frequency- and pattern-reconfigurable rhombic patch antenna with switchable polarization," *IEEE Antenna Wireless Propag. Lett.*, vol. 16, pp. 1639–1642, 2017.

[5] H. Sun and Z. Pan, "Design of a quad-polarization-agile antenna using a switchable impedance converter," *IEEE Antennas Wireless Propag. Lett.*, vol. 18, no. 2, pp. 269–273, Feb. 2019.

[6] F. Farzami, S. Khaledian, B. Smida, and D. Erricolo, "Pattern-reconfigurable printed dipole antenna using loaded parasitic elements," *IEEE Antennas Wireless Propag. Lett.*, vol. 16, pp. 1151–1154, 2017.

[7] C. R. White and G. M. Rebeiz, "Single- and dual-polarized tunable slot-ring antennas," *IEEE Trans. Antennas Propag.*, vol. 57, no. 1, pp. 19–26, Jan. 2009.

[8] T. Aboufoul, A. Alomainy, and C. Parini, "Reconfiguring UWB monopole antenna for cognitive radio applications using GaAs FET switches," *IEEE Antennas Wireless Propag. Lett.*, vol. 11, pp. 392–394, 2012.

[9] B. Ahn, H.-W. Jo, J.-S. Yoo, J.-W. Yu, and H. L. Lee, "Pattern reconfigurable high gain spherical dielectric resonator antenna operating on higher order mode," *IEEE Antennas Wireless Propag. Lett.*, vol. 18, no. 1, pp. 128–132, Jan. 2019.

[10] K. Van Caekenberghe and K. Sarabandi, "A 2-bit Ka-band RF MEMS frequency tunable slot antenna," *IEEE Antennas Wireless Propag. Lett.*, vol. 7, pp. 179–182, 2008.

[11] O. H. Karabey, S. Bildik, S. Bausch, S. Strunck, A. Gaebler, and R. Jakoby, "Continuously polarization agile antenna by using liquid crystal-based tunable variable delay lines," *IEEE Trans. Antennas Propag.*, vol. 61, no. 1, pp. 70–76, Jan. 2013.

[12] S. Bildik, S. Dieter, C. Fritzsch, W. Menzel, and R. Jakoby, "Reconfigurable folded reflectarray antenna based upon liquid crystal technology," *IEEE Trans. Antennas Propag.*, vol. 63, no. 1, pp. 122–132, Jan. 2015.

[13] K. K. Karnati, M. E. Trampler, and X. Gong, "A monolithically BST-integrated K_a-band beamsteerable reflectarray antenna," *IEEE Trans. Antennas Propag.*, vol. 65, no. 1, pp. 159–166, Jan. 2017.

[14] S. P. Srivastava, J. Handoo, K. M. Agrawal, and G. C. Joshi, "Phase-transition studies in n-alkanes and petroleum-related waxes—A review," *J. Phys. Chem. Solids*, vol. 54, no. 6, pp. 639–670, Jun. 1993.

[15] S. Himran, A. Suwono, and G. A. Mansoori, "Characterization of alkanes and paraffin waxes for application as phase change energy storage medium," *Energy Sources*, vol. 16, no. 1, pp. 117–128, Jan. 1994.

[16] E. T. Carlen and C. H. Mastrangelo, "Surface micromachined paraffin-actuated microvalve," *J. Microelectromech. Syst.*, vol. 11, no. 5, pp. 408–420, 2002.

[17] M. Lehto, R. Boden, U. Simu, K. Hjort, G. Thornell, and J.-Å. Schweitz, "A polymeric paraffin microactuator," *J. Microelectromech. Syst.*, vol. 17, no. 5, pp. 1172–1177, Oct. 2008.

[18] R. Bodén, M. Lehto, U. Simu, G. Thornell, K. Hjort, and J.-Å. Schweitz, "A polymeric paraffin actuated high-pressure micropump," *Sens. Actuators A, Phys.*, vol. 127, no. 1, pp. 88–93, Feb. 2006.

[19] B. Ghassemiparvin and N. Ghalichechian, "Complex permittivity measurement of paraffin phase-change material at 26 GHz–1.1 THz using time-domain spectroscopy," *J. Infr., Millim., THz Waves*, vol. 40, no. 2, pp. 210–218, Feb. 2019.

[20] B. Ghassemiparvin and N. Ghalichechian, "Reconfigurable millimeter-wave antennas using paraffin phase change materials," in *Proc. 10th Eur. Conf. Antennas Propag. (EuCAP)*, Apr. 2016, pp. 1–4.

[21] B. Ghassemiparvin, S. Shah, and N. Ghalichechian, "Novel paraffin-based 100-GHz variable capacitors for reconfigurable antennas," in *Proc. 11th Eur. Conf. Antennas Propag. (EUCAP)*, Mar. 2017, pp. 3506–3510.

Authorized licensed use limited to: Georgia Institute of Technology. Downloaded on January 12,2022 at 13:54:24 UTC from IEEE Xplore. Restrictions apply.

[22] B. Ghassemiparvin and N. Ghalichechian, "Paraffin-based RF microsystems for millimeter wave reconfigurable antennas," in *Proc. IEEE Int. Symp. Antennas Propag. USNC/URSI Nat. Radio Sci. Meeting*, Jul. 2019, p. 1.

[23] B. Ghassemiparvin and N. Ghalichechian, "Paraffin-based reconfigurable antenna operating at 100 GHz," *J. Microelectromech. Syst.*, vol. 29, no. 5, pp. 621–628, Oct. 2020.

[24] R. Garg, P. Bhartia, I. Bahl, and A. Ittipiboon, *Microstrip Antenna Design Handbook* (Antennas and Propagation Library). Norwood, MA, USA: Artech House, 2001.

[25] N. Behdad and K. Sarabandi, "A varactor-tuned dual-band slot antenna," *IEEE Trans. Antennas Propag.*, vol. 54, no. 2, pp. 401–408, Feb. 2006.

[26] N. Behdad and K. Sarabandi, "Dual-band reconfigurable antenna with a very wide tunability range," *IEEE Trans. Antennas Propag.*, vol. 54, no. 2, pp. 409–416, Feb. 2006.

[27] D. Pozar, *Microwave Engineering*, 4th ed. Hoboken, NJ, USA: Wiley, 2011.

[28] R. Simons, *Coplanar Waveguide Discontinuities and Circuit Elements*. Hoboken, NJ, USA: Wiley, 2002.

[29] L. J. Chu, "Physical limitations of omni-directional antennas," *J. Appl. Phys.*, vol. 19, no. 12, pp. 1163–1175, 1948.

[30] R. F. Harrington, "Effect of antenna size on gain, bandwidth, and efficiency," *J. Res. Nat. Bur. Standards D, Radio Propag.*, vol. 64D, no. 1, p. 1, Jan. 1960.

[31] R. C. Hansen, "Fundamental limitations in antennas," *Proc. IEEE*, vol. 69, no. 2, pp. 170–182, Feb. 1981.

[32] J. Choi *et al.*, "Frequency-adjustable planar folded slot antenna using fully integrated multithrow function for 5G mobile devices at millimeter-wave spectrum," *IEEE Trans. Microw. Theory Techn.*, vol. 68, no. 5, pp. 1872–1881, May 2020.

[33] Z. Jiang, S. M. Rahman, P. Fay, J. L. Hesler, and L. Liu, "Tunable 200 GHz lens-coupled annular-slot antennas using Schottky varactor diodes for all-electronic reconfigurable terahertz circuits," *Electron. Lett.*, vol. 49, no. 23, pp. 1428–1430, Nov. 2013.

[34] S. Hage-Ali, N. Tiercelin, P. Coquet, R. Sauleau, V. Preobrazhensky, and P. Pernod, "A millimeter-wave inflatable frequency-agile elastomeric antenna," *IEEE Antennas Wireless Propag. Lett.*, vol. 9, pp. 1131–1134, 2010.

[35] I. F. da Costa, S. A. Cerqueira, D. H. Spadoti, L. G. da Silva, J. A. J. Ribeiro, and S. E. Barbin, "Optically controlled reconfigurable antenna array for mm-wave applications," *IEEE Antennas Wireless Propag. Lett.*, vol. 16, pp. 2142–2145, May 2017.

[36] J. P. Dunsmore, *Handbook of Microwave Component Measurements*. Hoboken, NJ, USA: Wiley, 2012.

[37] L. Chen *et al.*, "Terahertz micromachined on-wafer probes: Repeatability and reliability," *IEEE Trans. Microw. Theory Techn.*, vol. 60, no. 9, pp. 2894–2902, Sep. 2012.

[38] *Understanding VNA Calibration*, Anritsu Company, Atsugi, Japan, 2012. Accessed: Nov. 30, 2019.

Authorized licensed use limited to: Georgia Institute of Technology. Downloaded on January 12,2022 at 13:54:24 UTC from IEEE Xplore. Restrictions apply.